Experimental Mechanics (2014) 54:743–752
DOI 10.1007/s11340-013-9846-y

Characterization of Laser Generated Lamb Wave Modes after Interaction with a Thickness Reduction Discontinuity Using Ray Tracing Theory

A. Balvantín · A. Baltazar · P. Rodriguez

Received: 3 May 2013 / Accepted: 27 December 2013 / Published online: 16 January 2014

Abstract The effect that a circular discontinuity (due to thickness reduction) in an Aluminum plate has on the direction of Lamb wave propagation was experimentally and theoretically studied. Broadband Lamb waves were generated by a pulsed Nd:YAG laser and optically detected with a photo-EMF detector to increase spatial resolution. The experimental results show that thickness reduction modifies the time of flight (TOF) for S0 and A0 vibration modes and generates a change in direction of the ultrasonic Lamb wave. The change in the TOF as a function of distance and thickness reduction was numerically determined using ray theory and then compared to experimental results. It is shown that the change in the direction of propagation depends on the vibrational mode and frequency of the Lamb waves and this can affect the detection and characterization of a hidden discontinuity.

Keywords Lamb waves · Laser-generated ultrasound · Photo-EMF detection · Ray tracing theory

Introduction

Accurate technology sensing and hidden defects characterization are critical tasks for structural health monitoring of engineering structures. Real time monitoring requires scanning large areas in a short period of time. The use of ultrasonic guided waves has been proposed as a potential method for discontinuity detection in engineering structures [1–4]. The study of guided waves and their practical implementation for structural health monitoring is complex due to dispersion phenomena and the existence of an infinite number of vibrational modes propagating in the media. The problem of dispersion and multiple modes associated with guided wave propagation has been addressed in several publications [3] and references therein. The number of modes that can be generated in a plate is a function of the frequency-thickness product. Due to the difficulties of identifying signal parameters, previous research focuses on the generation of a single mode of interest [5, 6].

Lamb waves are of particular interest due to their ability to propagate long distances in plates and pipe-like structures, offering a potential solution to defect detection in engineering structures [7]. Guided ultrasonic waves, such as Lamb waves, have recently been used for tomography reconstruction of discontinuities in plate-like structures [8–12]. However, mode conversion and ray path deviation phenomena are two of the main disadvantages associated with the application of Lamb waves to tomography reconstruction of hidden defects. The study of mode conversion of A0 and S0 modes after interaction with discontinuities has been reported [13–15]. It was found that even for these lowest modes, measurements of reflection coefficient from a notch-type discontinuity are difficult to perform due to mode conversion occurrence. Diffraction and refraction phenomena make it difficult to accurately identify the arrival time of a single Lamb wave mode of interest [16]. Ray tracing theory has been known to improve estimation of bulk ultrasonic signals' trajectory in tomography reconstruction [16–19].

The effect of a thickness reduction discontinuity on Lamb waves propagating in a media with multiple refractive indexes can be investigated using an experimental system with a high spatial resolution such as Laser ultrasonics [20]. In addition to high spatial resolution in the generation and acquisition of ultrasonic signals, the elimination of coupling problems, is another advantage of laser ultrasonics. The use of laser generated ultrasound for discontinuity detection has been previously reported in literature [21–25].

A. Balvantín · A. Baltazar (✉)
Robotics and Advanced Manufacturing Program, CINVESTAV, Unidad-Saltillo, Ramos Arizpe, Coahuila 25900, México
e-mail: arturo.baltazar@cinvestav.edu.mx

P. Rodriguez
INAOE, A.P.51, Puebla 72000, México

A pulsed laser can produce a broadband ultrasonic pulse in the plate; so multiple vibration modes are expected to be excited. Thus, complex behavior of Lamb waves requires advanced post processing techniques to allow accurate characterization of the ultrasonic signal. In this study, signals were post-processed by applying Fast Fourier Transform (FFT) spectrum, and Short-Time Fourier (STFT) analysis [26–28].

The goal of this work is to theoretically and experimentally study Lamb wave interaction with a circular thickness reduction discontinuity and its effects on A0 and S0 vibration modes; also, to further study the effect of ray bending, due to phase velocity changes in the area with the thickness reduction, on the discontinuity characterization.

Lamb Wave Propagation

Wave propagation of ultrasonic signals is correlated with the material properties of the studied media. When the propagating media has multiple refractive indexes, the differences between the properties of the materials cause the ultrasonic wave to not travel in a straight line. When an ultrasonic wave passes through an interface between two different velocities of a media at an oblique angle, both diffraction and refraction phenomena can take place.

Snell's Law describes the relationship between angles and velocities of waves passing through a boundary between two different isotropic media. To obtain TOF of ultrasonic signals, straight ray travel paths are not a good approximation for a signal propagating through a media with multiple refractive indexes or in anisotropic media [9]. A travel path of an ultrasonic signal that connects a transmitter-receiver pair is referred to as linking ray. The ideal condition for determination of the TOF is when signals propagate through a single linking ray. However, unidirectional beams that propagate through an anisotropic media or a media with multiple refractive indexes, may not reach the receiver position (see Fig. 1(a)). Omnidirectional transducers guarantee the existence of at least one linking ray between the transducers in a media with multiple refractive indexes (see Fig. 1(b)).

Lamb waves are symmetric and antisymmetric acoustic waves [29] propagating along thin plates. Since the ultrasonic signal wavelength is of the order of the plate thickness d, the Lamb waves are dispersive for finite values of the ratio of the Lamb wavelength λ and d. A main advantage of ultrasonic Lamb waves is their ability to propagate long distances in a structure. On the contrary, multiple dispersion modes generated in the propagating media are a disadvantage of Lamb waves as an affective discontinuity characterization technique.

Rayleigh-Lamb frequency equations are used to calculate theoretical Lamb wave dispersion curves:

$$\frac{\tan(qh)}{\tan(ph)} = -\frac{4k^2pq}{\left(q^2-k^2\right)^2}, \frac{\tan(qh)}{\tan(ph)} = -\frac{\left(q^2-k^2\right)^2}{4k^2pq}, \tag{1}$$

$$p^2 = \left(\frac{\omega}{c_L}\right)^2 - k^2, q^2 = \left(\frac{\omega}{c_S}\right)^2 - k^2, k = \frac{\omega}{c_p}, \text{ and } c_p = \left(\frac{\omega}{2\pi}\right)\lambda, \tag{2}$$

where k is the wave number, c_L and c_S are the longitudinal and shear bulk velocities respectively c_p is the phase velocity of the Lamb wave mode, ω is the circular frequency and h is the thickness of the plate (d) divided by two.

Group velocity could be obtained from phase velocity by using the following expression:

$$c_g \equiv \frac{d\omega}{dk}, \omega = c_p k \rightarrow c_g = c_p + k\frac{dc_p}{dk}, \tag{3}$$

where k is wave number.

Theoretical dispersion curves (Fig. 2) show phase and group velocities as a function of frequency. Lowest order vibrational modes, A0, A1, S0 and S1 for the propagation parameters of the sample plate are given. These curves can be used for mode identification of the captured ultrasonic signals.

A0 and S0 are the only fundamental Lamb wave modes that exist at low frequency range. Lowest order dispersion modes are also easy to identify, and for this reason they are frequently used in practical nondestructive testing. In this work, the effect of a circular thickness reduction discontinuity on A0 and S0 propagation modes is studied.

A thickness reduction causes variations in the propagation velocities of the Lamb waves, generating a corresponding change in the acoustic impedance of the regions with a different thickness value. Here, synthetic regions where the vibrational modes have phase velocity values higher (fast velocity region) and lower (slow velocity region) than the propagation velocity of the sample plate are used to study the effect of a

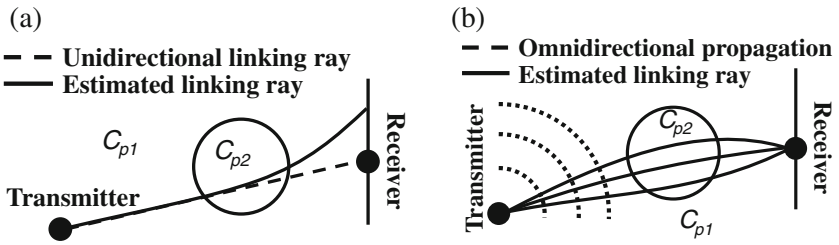

Fig. 1 Unidirectional (**a**) and omnidirectional (**b**) wave propagation for a transmitter-receiver pair. A *circular area* with phase velocity C_{p2} is embedded in a media with phase velocity C_{p1}

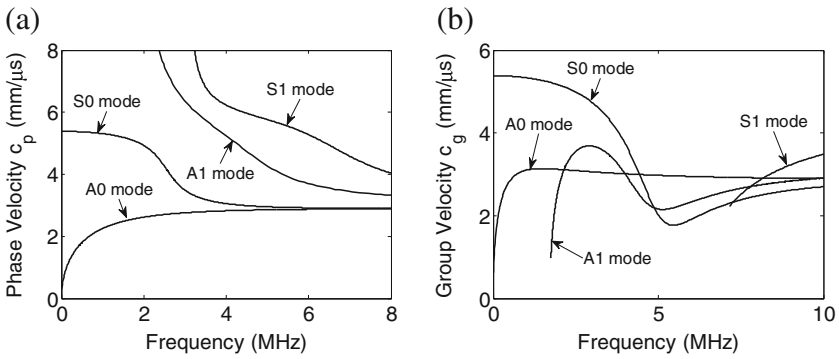

Fig. 2 Theoretical dispersion curves for a 0.9 mm thick Aluminum plate; (**a**) phase and (**b**) group velocity

thickness reduction discontinuity in the Lamb wave propagation paths. This phenomenon has been studied for artificial inclusions and bulk waves using ray tracing theory [11, 16–19]. It was found that in the presence of material discontinuities, ray tracing algorithms provide a better approximation of the time of flight (TOF) of bulk ultrasonic signals than do the straight ray assumption predictions.

Slowness Distribution Function

To numerically evaluate the sensitivity of Lamb wave modes on thickness reduction discontinuity, a synthetic slowness distribution function *f(x,y)* was generated with the corresponding phase velocity (c_p) value for each dispersion mode. Figure 3 shows the phase and group velocity dispersion curves for both modes A0 and S0 propagating in plates with two different thickness values. A synthetic slowness distribution is generated from the c_p values of an aluminum plate (0.9 mm in thickness) and the circular region (thickness reduction discontinuity) with a 0.45 mm in thickness at a frequency value of 1.5 MHz (vertical dashed line in Fig. 3(a)). At this frequency, the change in value of phase velocity as a function of the thickness variation for both vibrational modes is noticeable. Phase velocity (c_p) of the S0 mode is equal to 5.19 mm/μs for a thickness of 0.9 mm and 5.34 mm/μs for 0.45 mm. For A0 mode, phase velocity is 2.49 mm/μs for 0.9 mm and 2.07 mm/μs for 0.45 mm.

Figure 4 shows the synthetic *f(x,y)* distribution for both dispersion modes S0 and A0. The *f(x,y)* distribution in Fig. 4 represents a plate with an area of 100×45 mm and a circular thickness reduction discontinuity of 9.5 mm in radius.

In Fig. 4, phase velocity for S0 mode is higher in the plate than in the discontinuity area and the opposite can be seen for A0 mode. It can also be seen that for a limited number of ten transmitter and receivers (10×10 grid), a low resolution approximation to the circular thickness reduction defect is obtained (Fig. 4(a) and (b)). A denser grid for the discretization process (see Fig. 4(c) and (d)) improves the numerical approximation to the geometry of the discontinuity but it also increases the computational cost as will be discussed in the following sections.

Ray Tracing Modeling

Ray tracing theory describes a method for calculating the path of elastic waves through an object having regions with varying wave propagation velocity. Material discontinuities and anisotropy could produce variations in the propagation parameters of a media. Ultrasonic waves traveling through this kind of media could suffer a deviation at every interface between material zones of different acoustic impedance. As a result of this deviation, the path is curved and ultrasonic rays no longer travel in straight trajectories from transmitter to receiver transducer.

Several approximate theories have been proposed in literature to solve the ray bending problem. [17, 18, 30] proposed

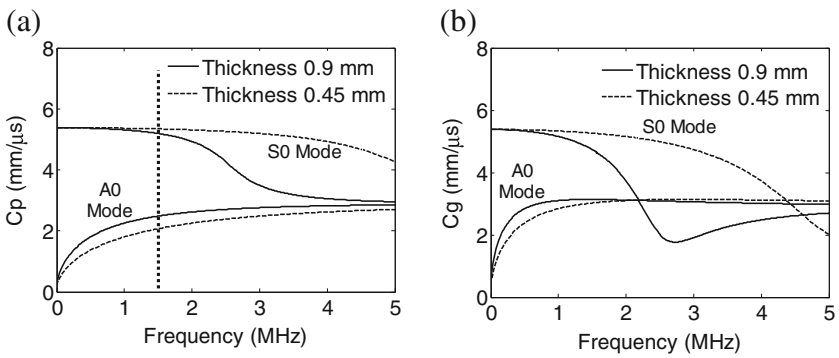

Fig. 3 Theoretical dispersion curves for the S0 and A0 modes with different thickness values. (**a**) Phase velocity; (**b**) group velocity

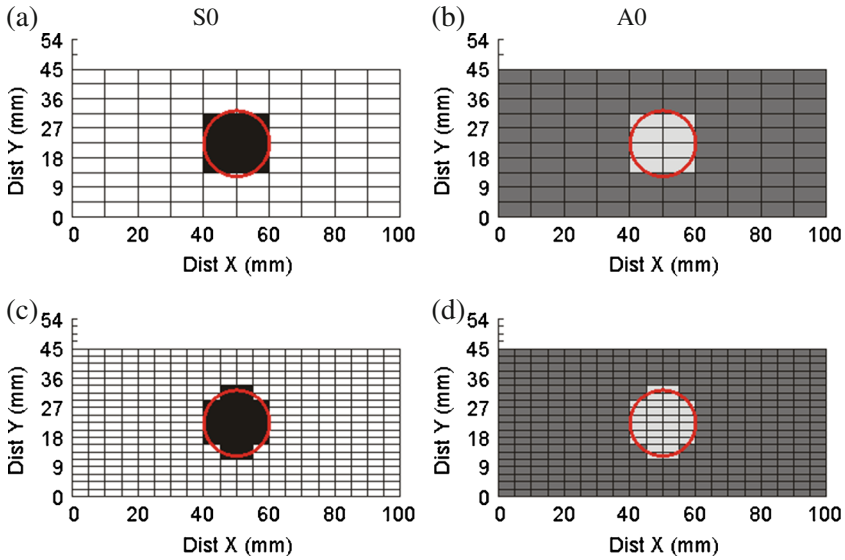

Fig. 4 Synthetic slowness distribution *f(x,y)* of S0 and A0 modes obtained using the values of phase velocity for plate and discontinuity with different grid densities: (**a**), (**b**) 10×10, (**c**), (**d**) 20×20

algorithms based on the Fermat principle which states that the energy of rays propagates along the trajectories of minimum time of flight (TOF). Ray tracing algorithms have recently been used to improve numerical models in practical implementations. Connolly et al. [9] developed a numerical model based on the spatial variation of material properties found in welds to compute delay laws to trace the ray travel paths in nonhomogeneous and anisotropic propagation media. Denis et al. [31] implemented a ray tracing algorithm based on the eikonal equation to perform ultrasound transmission tomography in refracting media. However, the modeling of Lamb wave propagation using ray tracing theory still needs to be further studied.

If we assumed that the ray travel path of an ultrasonic signal can be determined by modeling the propagation media as a sampled grid of constant material properties in each cell (see Fig. 5); then, the ray incident at a point of the sampled grid *f(x,y)*, follows a trajectory that is described by Snell's law:

$$\frac{\sin(\alpha+d\alpha)}{c_p+dc_p}=\frac{\sin(\alpha)}{c_p}, \tag{4}$$

where c_p is the phase velocity and α is the angle between the tangent to the ray and the gradient of the velocity ∇c_p at any point in the travel path.

Figure 5, *f(x,y)* exemplifies a discrete distribution of slowness (*1/c_p*); w_{ij} is the amount of ray that traveled in a determined cell of the discrete distribution *f(x,y)*; Δx and Δy are the cell size of *f(x,y)* in the X_i and Y_j axis respectively. The TOF for each ray can be obtained using the following relationship:

$$V=\frac{d}{t}\rightarrow T_{OF}=fw, \tag{5}$$

where V is phase velocity; d is distance; t is time; T_{OF} is the time of flight of the ray and $f=1/c_p$.

The relationships between two adjacent points of the travel path are determined by:

$$\cos(\alpha)=\frac{\left(\frac{\partial c_p}{\partial x}a_x+\frac{\partial c_p}{\partial y}a_y\right)\cdot\left(dxa_x+dya_y\right)}{\left|\frac{\partial c_p}{\partial x}a_x+\frac{\partial c_p}{\partial y}a_y\right|\left|dxa_x+dya_y\right|},$$
$$\sin(\alpha)=\frac{\left(\left(\frac{\partial c_p}{\partial x}a_x+\frac{\partial c_p}{\partial y}a_y\right)\times\left(dxa_x+dya_y\right)\right)\cdot a_z}{\left|\frac{\partial c_p}{\partial x}a_x+\frac{\partial c_p}{\partial y}a_y\right|\left|dxa_x+dya_y\right|}, \tag{6}$$

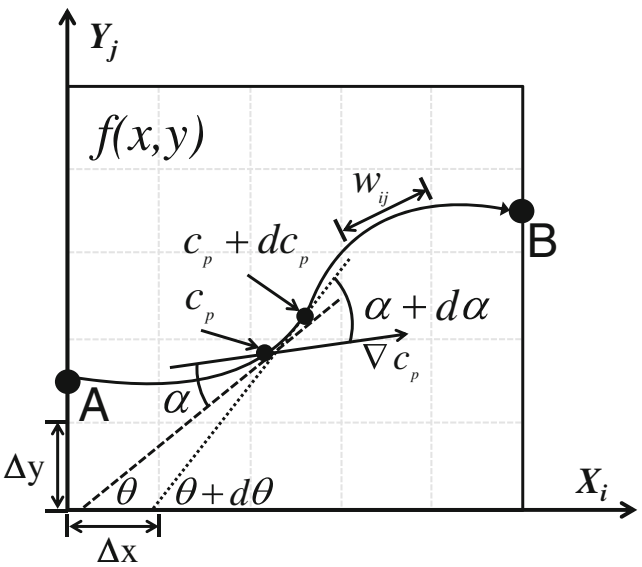

Fig. 5 Snell's law for two points of the signal travel path

where (a_x,a_y,a_z) are unit vectors in the x, y, z directions, $d\alpha=d\theta$, and $dc_p=((\partial c_p/\partial x)a_x+(\partial c_p/\partial y)a_y)\cdot(dxa_x+dya_y)$.

From equation (6) the following ray equation can be obtained, see [17] for a detailed description:

$$\frac{d\theta}{dx}=\frac{1}{c_p}\left(\frac{\partial c_p}{\partial x}\frac{\partial y}{\partial x}-\frac{\partial c_p}{\partial y}\right). \tag{7}$$

If $f=1/c_p$, $\tan(\theta)=y_x^{'}$, and $d\theta/dx=y_x^{''}/(1+y_x^{'2})$ the ray equation can be established as follows:

$$y_x^{''}=\frac{1}{f}\left(\frac{\partial f}{\partial y}-\frac{\partial f}{\partial x}y_x^{'}\right)\left(1+y_x^{'2}\right), \tag{8}$$

where f is the slowness value of the propagation media.

The ray path expressed in function of the Y_j axis (see Fig. 5), $y(x)$, can be described as:

$$y_x^{''}=\frac{y_{k+1}-2y_k+y_{k-1}}{i_x^2}, \tag{9}$$

where i_x is the step in the ray travel path.

The discrete form of the ray equation, for numerical implementation can now be obtained by combining equations (8) and (9):

$$y_{k+1}=2y_k-y_{k-1}+\frac{i_x^2}{f(x_k,y_k)}\left(\frac{\partial f}{\partial y}-\frac{\partial f}{\partial x}y_k^{'}\right)\left(1+y_k^{'2}\right), \tag{10}$$

where $y_k^{'}=(y_k-y_{k-1})/i_x$.

Bilinear interpolation Denis et al. [31] can be used to calculate the derivatives of the slowness distribution at each step in the ray travel path:

$$\begin{aligned}\frac{\partial f}{\partial x}&=\frac{f(x_k,y_k)-f(x_{k-1},y_k)}{i_x},\\ \frac{\partial f}{\partial y}&=\frac{f(x_k,y_k)-f(x_k,y_{k-1})}{y_k-y_{k-1}}.\end{aligned} \tag{11}$$

From the previous theory it is possible to establish the following ray tracing algorithm.

Given an initial y_i coordinate (transmitter transducer position) and a corresponding shooting angle θ, trace the complete ray travel path to obtain the final y_f coordinate (receiver transducer position) using equation (10).

Calculate the time of flight for the obtained ray path by multiplying the fragment of the travel path (w_{ij}) and the $f(x,y)$ value at each cell.

Establish a range for the shooting angle θ and repeat steps (a) and (b) until the minimum TOF for the calculated ray path is obtained.

Change the initial y_i coordinate and repeat (a)-(c).

Rays with minimum TOF provide with an improved approximation of the straight ray assumption to the actual ultrasonic signal trajectory between the transmitter-receiver pair. To compare with TOF experimentally measured from STFT, group velocity was used in equation (5) instead of phase velocity.

Numerical calculations using the above methodology for ray tracing of Lamb wave propagation through a slowness distribution describing a circular discontinuity is shown in Fig. 6. In these calculations the low density grid is based only on ten receiver/transmitters positions (Fig. 6(a) and (b)).

Figure 6 shows that the fast velocity region (S0 mode) slightly affects the trajectory of the ray propagation direction; while the effect is greater for the slow velocity region (A0 mode). The comparison of straight ray TOF with results of time of flight based on ray tracing obtained with equation (5), using phase and group velocity, are given in Fig. 7. S0 mode exhibits only a minimal difference between phase and straight arrival time and a more noticeable difference of group TOF with respect to straight ray TOF. On the other hand, A0 mode exhibits nominally equal arrival times for straight and group TOF. This phenomenon is explained by the inverse effect of thickness variation on phase and group velocity of A0 and S0 modes (see Fig. 3).

Ray tracing theory predicts that the slow velocity region would obstruct the propagation of ultrasonic signal at receiver position S7 (Fig. 6(b)). The behavior of Lamb waves in the presence of a slow velocity region is similar to the results with

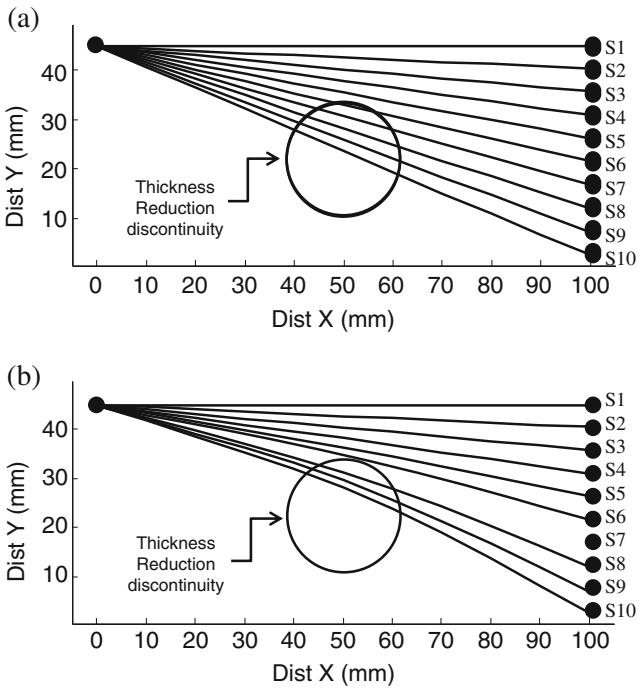

Fig. 6 Ray tracing approximation for direction of propagation of (**a**) S0 mode (with fast velocity region) and (**b**) A0 mode (slow velocity region)

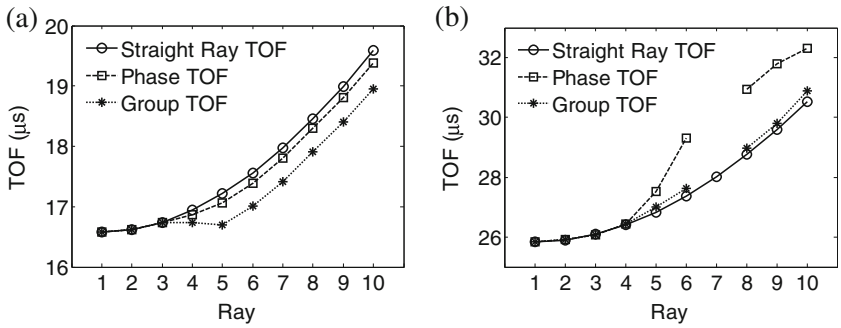

Fig. 7 Numerical TOF estimation for (**a**) S0 and (**b**) A0 mode

bulk waves reported by [16]. It should be noticed that the almost unperceivable bending in ray #6 for A0 mode, which passes near the discontinuity but not over it, is a consequence of the low resolution of the grid used for the calculations (see Fig. 4(a)).

To corroborate the numerical findings, experiments using an aluminum plate with an artificially machined thickness-reduction discontinuity were performed. A pulsed laser and a photo-electromotive force detector were used for generation and data capture processes of ultrasonic signals. Laser generated ultrasound was implemented to increase spatial resolution of ultrasonic rays for the data gathering process.

Experimental Setup and Results

The experimental setup for detecting the laser-generated Lamb waves using the photo-EMF detector is depicted in Fig. 8. The photo-EMF detector used was a GaAs crystal with frontal dimensions of 3×3 mm and 0.5 mm thick. The sensitive area of the detector was limited by two stripe gold electrodes with a spacing of ≈ 300 μm. A Distributed Bragg Reflector (DBR) laser diode with a continuous wave output power of ≈ 90 mW at wavelength emission of 852 nm was used as a probe laser. The laser beam was split into two beams,

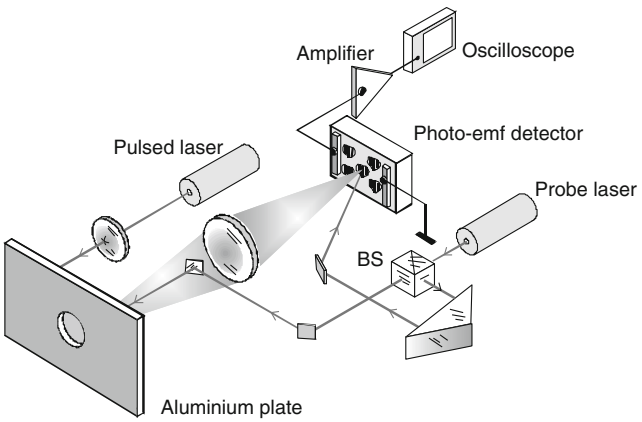

Fig. 8 Experimental setup to detect laser-generated Lamb waves by a photo-EMF detector

one of them inspected the test sample and the backscattered light was collected and brought into interference with the second (reference) beam at the photo-EMF detector. Small ultrasonic vibrations on the sample test produced lateral displacements of the interference pattern. As a consequence of these fast displacements, an electrical current was generated through the photo-EMF detector, which is closely related to the vibrations on the sample surface [32]. The photo-EMF electrical current was amplified by a transimpedance amplifier (30 MHz bandwidth and 1 MΩ gain) and observed and stored in a digital oscilloscope with a frequency band of 20 MHz. The ultrasonic waves were generated by a Nd:YAG pulsed laser (10 ns pulse width and ≈ 500 mJ of energy per pulse). A cylindrical lens, of 25 cm focal length, focused the laser beam on a line 200 μm wide and 1 cm long. The test sample was an aluminum plate with dimensions of 220×110 mm and 0.9 mm thick. A circular discontinuity (r≈9.5 mm and 0.45 mm in depth) was machined on the back side of the plate. The sample plate was assumed to be isotropic; no indication of anisotropy was measured during the experiments.

The accuracy of the experimental system depends on the precise location of the transmitter-receiver pairs. Experimental signals were acquired by changing the position of the pulsed laser and fixing the sample plate for a single projection and also by capturing signals from parallel positions of the transmitter receiver pair. Signals were acquired using the proposed experimental set-up with a maximum resolution of 0.1 μs.

The area around the defect was scanned using the scheme depicted in Fig. 9. The pulsed laser was aimed to position t1 and t5 on the aluminum plate and the probe laser receiver at ten different positions (s1-s10) on the opposite side of the plate. The horizontal linear distance between the lines of transmitter and receiver transducers was set to 100 mm and the distance between the first and tenth positions of the transducers was set to 45 mm. The high spatial resolution of the experimental system as compared with standard contact transducers (typically 12.7 mm in diameter) allows the generation and capture processes of the ten rays (profile) in a small region around the discontinuity. Profiles of signals generated with the transmitter sensor (t) in the first and fifth positions (Fig. 9) were used to describe the interaction of Lamb waves with the

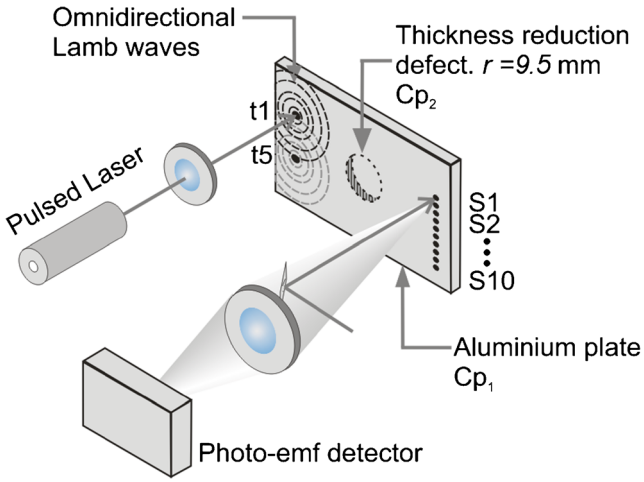

Fig. 9 Depiction of the scheme for data gathering process for the first (*left*) and fifth (*right*) positions of the pulsed laser (*t1*, *t5*). The distance between laser and detector in the t1-s1 pair is 100 mm; the distance between receiver positions (s1,s2…s10) is 4.5 mm

thickness reduction discontinuity. These profiles provide information of the normal and oblique interaction of Lamb waves with the discontinuity.

Estimation of time of flight was obtained by setting a frequency value of interest (1.5 MHz) and plotting the profile of the spectrogram (STFT) on the time-spectrum amplitude axis. It is known that FFT can be used to determine which frequencies are present in the captured signal, but the information on the time reference for those frequencies cannot be obtained [27]. On the other hand, STFT evaluates the time-domain signal into a series of small time intervals, each is windowed and the Fourier transform is applied individually for each one and then put together to produce a spectrogram of the signal. The time of flight can be determined by identifying the maximum amplitude of the spectrogram profile at a time window around each mode [33].

Figure 10(a), (c) and (e) show the captured time domain signals for different locations of the photo EMF detector with the transmitter sensor aimed at position 1. The time signal was

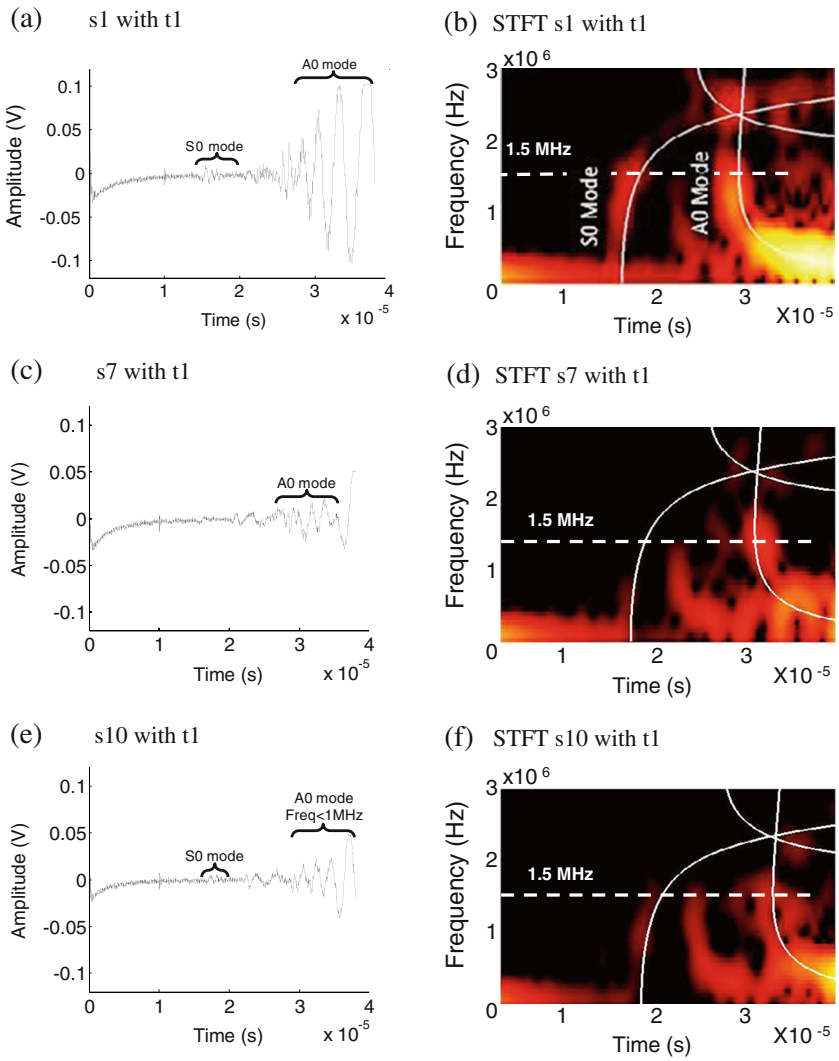

Fig. 10 Time-domain signals (*left*) and their STFT (*right*) generated by the pulsed-laser excitation line at position t1 and detected by the photo-EMF detector located on the opposite side at position s1, s7 and s10

averaged over 32 shots in order to improve the signal to noise ratio. In Fig. 10(a), a typical time-domain signal away from the region with the thickness reduction discontinuity (transmitter and receiver at position 1) is shown. The corresponding spectrogram is given in Fig. 10(b). For comparison purposes, the theoretical dispersion curve for a plate (0.9 mm in thickness) is superimposed onto the experimental one. It is observed that both S0 and A0 dispersion modes are received when there is not interaction with the discontinuity (Fig. 10(b)). Thus, arrival of S0 and A0 modes are clearly identified. The observed signal pattern in-between A0 and S0 is the result of reflections in the edges of the plate.

Our interest here is on the arrival time as affected by ray bending at the discontinuity of S0 and A0 at the frequency of 1.5 MHz. The effect of mode conversion on the strength of these modes was not studied. It was found that for a receiver located in position 7 and 10, the interaction with the discontinuity distorts the captured Lamb wave signals. This effect is more evident in the time-frequency representations of the ultrasonic signals, which shows that the receiver at position 7 does not detect S0 mode at the frequency of 1.5 MHz used in the theoretical predictions based on ray theory (see Fig. 6). For sensor at position 10, S0 and A0 are again detected; however, the TOF of A0 mode cannot be accurately determined due to low signal to noise ratio (Fig. 10(f)). Therefore, once the wave propagates over the discontinuity region, A0 and S0 are affected differently as a function of the excitation frequency. This phenomenon can be explained by the varying incidence angle relative to the receiver/transmitter position and to the position and thickness of the discontinuity. Therefore, these

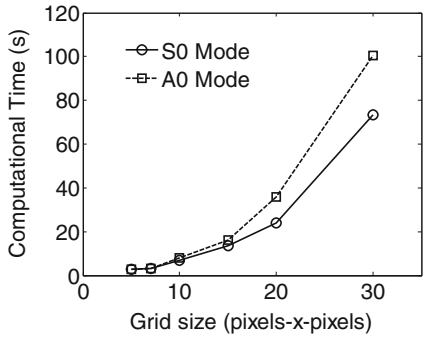

Fig. 12 Computational time for different grid sizes of the slowness distribution *f(x,y)*

results corroborate the expected effect of the discontinuity as a function of the incidence angles on S0 or A0 vibrational mode as predicted by the ray theory.

The numerical calculations of time of arrival (TOF) estimation using straight ray and ray tracing approximations are given in Fig. 11 together with experimental measurements (asterisks). It can be seen that experimental measurements agree better with ray tracing approximation (circles) than with straight ray assumption (solid line). If the transmitter is located at position 1, S0 mode is not detected at 1.5 MHz by the receiver in positions 6, 7 and 9 (Fig. 11(a)). Similar results were obtained for experimental measurements of A0 in receiver positions 5, 6 and 10 (Fig. 11(b)). As predicted, the slow and fast velocity regions defined by the phase velocities of A0 and S0 modes influence experimental measurements by making S0 mode more sensitive than A0 mode to the thickness reduction discontinuity. This outcome, apparently in

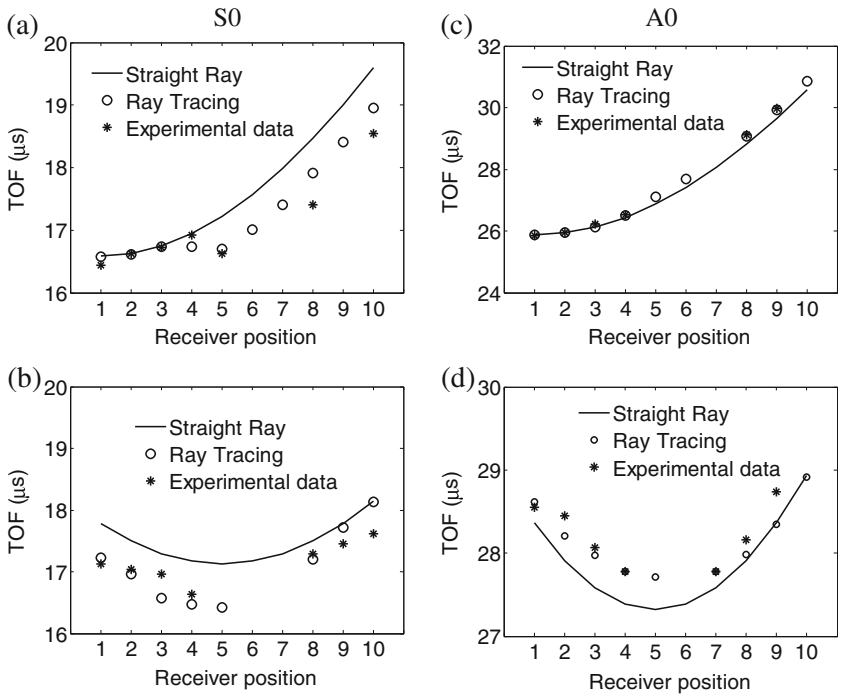

Fig. 11 Time of flight TOF profile, showing theoretical straight ray and ray tracing approximations and also experimental measurements for S0 (*left*) and A0 mode (*right*), taken at t1 (**a** and **c**); and t5 (**b** and **d**)

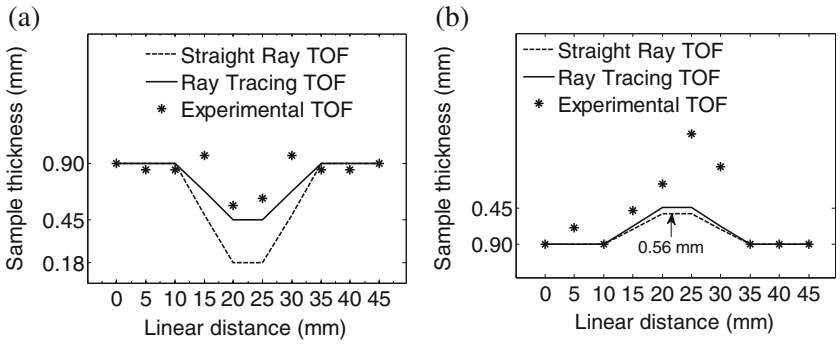

Fig. 13 Thickness profiles reconstructed from parallel rays in the transmitter/receiver pair for (**a**) S0 mode; (**b**) A0 mode

contradiction with the large ray bending effect observed for A0, can be explained by the difference in values of group velocity for these two modes (see Fig. 7). For example, in the case of A0 mode, the larger trajectories due to ray bending are compensated by the high group velocity at the discontinuity region resulting in equal TOF for ray tracing and straight ray. For S0, the lower group velocity at the discontinuity region is responsible for the observed difference between straight and ray tracing TOF. Finally, we can say that despite the fact that the discretization of the 10×10 grid used in the numerical calculations was relatively low, ray tracing results and experimental findings agree quite well.

A poor discretization of the sample plate reduces the resolution in ray tracing approximation; however, the implementation of a grid with a large number of cells to model *f(x,y)* will increase the computational cost of the ray tracing algorithm. In the numerical measurements a 10×10 grid was used to discretize the shape of the discontinuity in the sample plate in order to keep a low computational cost. As shown in Fig. 12, numerical calculations with a high resolution grid will significantly increase the computational time for both modes.

Figure 13 shows the profiles generated by S0 and A0 modes at 1.5 MHz. These profiles were obtained at parallel positions (t1-s1, t2-s2… t10-s10) of the transmitter-receiver pair (see Fig. 9). There, lines are the numerically calculated thickness values using ray theory and straight ray and scatter points are the experimental results. Clearly, ray theory approaches actual thickness values of the defect (0.45 mm); thus, direct observation of these profiles can be used as a rough estimate of the size of the defect which can be improved if a high number of parallel rays is applied.

Numerical and experimental results show that detection and characterization of a discontinuity, depends not only on a proper selection of a single vibration mode but also on the frequency range. The numerical approximation implemented in this work can be used to obtain an approximation of discontinuity dimensions. A numerical approximation of Lamb wave propagation could help to optimize the experimental set up, based on the proper selection of the Lamb wave mode, sensor locations and frequencies. Also, experimental data gathering process could be improved by numerically establishing the correct incidence angle at which a specific dispersion mode of interest can be used to detect a discontinuity.

Conclusions

In this work, the interaction of laser generated ultrasonic Lamb waves with a thickness reduction discontinuity was experimentally and numerically studied. Experiments were performed on a 0.9 mm thick aluminum plate having an artificially machined with 50 % circular thickness reduction discontinuity of 19 mm in diameter. Numerical calculations used synthetic *f(x,y)* slowness distributions generated from theoretical dispersion curves of S0 and A0 modes. It was found that the thickness variation at the discontinuity region along with the frequency values determines the sensitivity of a dispersion mode to the thickness reduction discontinuity. Comparison between experimental and numerical results shows that the photo-EMF laser detector provides enough spatial resolution and signal to noise ratio to observe ray bending of Lamb waves. Results of this work show the potential use of ray tracing theory to model the interaction of Lamb waves with a thickness reduction defect. The proposed methodology could be used to improve tomography reconstruction based on ray tracing TOF for accurate discontinuity characterization.

Acknowledgments This work was sponsored by CONACYT grant SEP-CONACYT 58951.

References

1. Cawley P, Lowe MDJ, Alleyn DN, Pavlakovic B, Wilcox P (2003) Practical long range guided wave testing: application to pipes and rail. Mater Eval 61:66–74
2. KunduT (2004) Ultrasonic nondestructive evaluation: engineering and biological material characterization. CRC press
3. Rose JL (1999) Ultrasonic waves in solid media. Cambridge University Press

4. Rose JL (2004) Ultrasonic guided waves in structural health monitoring. Adv Nondestruct Eval 270:14–21
5. Alleyne D, Cawley P (1996) The use of Lamb waves for the long range inspection of large structures. Ultrasonics 34:287–290
6. Tua PS, Quek ST, Wang Q (2004) Detection of cracks in plates using piezo-actuated Lamb waves. Smart Mater Struct 13:643–660
7. Dalton RP, Cawley P, Lowe MJS (2001) The Potential of Guided Waves for Monitoring Large Areas of Metallic Aircraft Fuselage Structure. J Nondestruct Eval 20:29–46
8. Balvantin A, Baltazar A, Kim JY (2010) Ultrasonic lamb wave tomography of non-uniform interfacial stiffness between contacting solid bodies. In AIP Conference Proceedings, Vol., 1211, pp 1463-1470
9. Connolly GD, Lowe MJS, Temple JAG, Rokhlin SI (2010) Correction of ultrasonic array images to improve reflector sizing and location in inhomogeneous materials using a ray-tracing model. J Acoust Soc Am 127:2802–2812
10. Leonard KR, Malyarenko EV, Hinders MK (2002) Ultrasonic lamb wave tomography. Inverse Problems 18:1795–1808
11. Malyarenko EV, Hinders MK (2001) Ultrasonic Lamb wave diffraction tomography. Ultrasonics 39:269–281
12. McKeon JC, Hinders MK (1999) Parallel projection and crosshole Lamb wave contact scanning tomography. J Acoust Soc Am 106: 2568–2577
13. Lowe MJS, Cawley P, Kao J-Y, Diligent O (2002) The low frequency reflection characteristics of the fundamental antisymmetric Lamb wave a_0 from a rectangular notch in a plate. J Acoust Soc Am 112: 2612–2622
14. Diligent O, Grahn T, Boström A, Cawley P, Lowe L (2002) The low-frequency reflection and scattering of the S0 Lamb mode from a circular through-thickness hole in a plate: Finite Element, analytical and experimental studies. J Acoust Soc Am 112:2589–2601
15. Fromme P, Wilcox P, Lowe MJS, Cawley P (2004) On the scattering and mode conversion of the A0 lamb wave mode at circular defects in plates. In AIP Conference Proceedings, Vol 700. pp 142-149
16. Andersen AH (1990) Ray tracing for reconstructive tomography in the presence of object discontinuity boundaries: a comparative analysis of recursive schemes. J Acoust Soc Am 89:574–582
17. Andersen AH, Kak AC (1982) Digital ray tracing in two-dimensional refractive fields. J Acoust Soc Am 72:1593–1606
18. Pereyra V (2000) Ray tracing methods for inverse problems. Inverse Probl 16:R1–R35
19. Wang B, Takatsubo J, Toyama N, Akimune Y, Zhao M (2006) An improved ray tracing algorithm for ultrasonic CT in nondestructive inspections. ICSP Proc 1:5–8
20. Scruby CB, Drain LE (1990) Laser ultrasonics: techniques and applications. Adam Hilger, Bristol
21. Benz R, Niethammer M, Hurlebaus S, Jacobs L (2003) Localization of notches with Lamb waves. J Acoust Soc Am 114:677–685
22. Birnbaum G, White G (1984) Laser techniques in NDE, vol 7, Research techniques in nondestructive testing. Academic Press, New York
23. Kim DY, Lee SJ, Lee JH (2008) Application of laser-generated ultrasound for evaluation of wall-thinning in carbon steel elbow. In 17th World Conference on Nondestructive Testing, pp 25–28
24. Park JH, Lee JH, Seo GC, Choi SW (2006) Application of laser-generated ultrasound for evaluation of thickness reduction in carbon steel pipes. Key Eng Mater 321:743–746
25. Wu CH, Yang CH (2011) Laser ultrasound technique for ray tracing investigation of Lamb wave tomography. In SPIE Smart Structures and Materials + Nondestructive Evaluation and Health Monitoring. International Society for Optics and Photonics, pp 79833L–79833L
26. Cohen L (1995) Time frequency analysis, Prentice Hall. Upper Saddle River, New Jersey
27. Flandrin P (1999) Time-frequency/time-scale analysis, wavelet analysis and its applications, vol 10. Academic Press, San Diego
28. Mallat S (1999) A wavelet tour of signal processing. Academic Press, CA
29. Cheeke JDN (2002) Fundamentals and applications of ultrasonic waves. CRC Press
30. Berryman JG (1989) Fermat's principle and nonlinear traveltime tomography. Phys Rev Lett 62:2953–2956
31. Denis F, Basset O, Gimenez G (1995) Ultrasonic transmission tomography in refracting media: reduction of refraction artifacts by curved-ray techniques. IEEE Trans Med Imaging 14:173–188
32. Rodriguez P, Stepanov S, Wang CC, Trivedi S (2006) Laser ultrasound detection by CdTe:V monopolar photo-EMF detector with responsivity close to theoretical limit. Nondestruct Test Eval 21:95–102
33. Alleyne D, Cawley P (1991) Two-dimensional Fourier transform method for the measurement of propagating multimode signals. J Acoust Soc Am 89:1159–1168